# Onset of bioconvection in suspensions of *Bacillus subtilis*

Imre M. Jánosi,[1,2] John O. Kessler,[3] and Viktor K. Horváth[4]
[1]*Department of Physics of Complex Systems, Eötvös University, Múzeum körút 6-8, H-1088 Budapest, Hungary*
[2]*Höchstleistungsrechenzentrum (HRLZ), Forschungszentrum Jülich, D-52425 Jülich, Germany*
[3]*Department of Physics, University of Arizona, Tucson, Arizona 85721*
[4]*Department of Biological Physics, Eötvös University, Puskin utca 5-7, H-1088 Budapest, Hungary*
(Received 19 March 1998)

Bioconvection occurs when upward swimming micro-organisms generate gravitational energy that initiates and maintains dissipative movement of the water in which they swim. Advection, and motion of the organisms relative to the fluid, generate patchiness in concentration that drives and shapes the geometry and rate of convection. This paper presents a method for quantitatively analyzing the development of self-organization, and numerical estimates that connect and interpret theory and experiment. While the oxygen consuming, oxgen-gradient-guided bacteria *Bacillus subtilis* are the sole subject here, the methods developed will find application to the analysis and modeling of other complex dynamic systems that ineluctably combine physics and biology. [S1063-651X(98)01210-0]

PACS number(s): 87.45.−k, 47.20.−k, 47.54.+r

## I. INTRODUCTION

Populations of algae or bacteria swimming in a quiescent body of water often generate the collective phenomenon called ''bioconvection'' [1–16]. In fully developed bioconvection, the mean local concentration (and sometimes also the swimming direction [6]) of the organisms is coupled to the local fluid velocity of the convection cells. As in thermally driven convection, the continuous motion of the fluid is due to the nonuniformity of its mean density. In thermal convection this nonuniformity is supplied by heat flux through the boundaries. In bioconvection, which is isothermal, the nonuniformity of the density is generated and maintained by the directional swimming of the ''heavy'' organisms suspended in the fluid. They are advected with the fluid and also swim relative to it.

Bioconvection is of intrinsic interest because it is based on dynamic synergism between physics and biology: (1) Individual swimming micro-organisms convert energy available at low concentration into growth, division, and power for motion. (2) The organisms possess and use sensory apparatus for guidance toward improving or more appropriate environments. (3) Individual organisms interact with the local and remote physical world through viscosity and gravity. (4) The suspension, of organisms and water, is subject to fluid dynamics and constraints at the boundaries. (5) The motional and concentrative dynamics of the suspension are driven by anisotropy generated by behavior that depends in part on these dynamics. (6) The behavior of the micro-organisms is not deterministic, but can be modeled by probability density functions.

It is not difficult to write a set of equations governing some idealized version of all that. However, solving this coupled nonlinear set comprising Navier-Stokes, organism conservation, and molecular species conservation is another matter. Various approaches to them, through linear and weakly nonlinear stability theory [9,13,14] and through a closed form solution of a severely idealized versions [6,7], have been published. Furthermore, there has not been much quantitative analysis of experiments available for testing any theoretical developments that might become available.

In this paper the onset of the bioconvective instability is analyzed by laboratory experiments on cultures of bacteria. We measured the delay time $T$ for pattern formation in concentrated suspensions of swimming bacteria. $T$ is the time interval from a homogeneous mixed initial condition to the appearance of nonuniformity in cell concentration, immediately preceding the start of convective patterns. We found that this time does not depend on the diameter of the container and the depth of the liquid layer. The important parameters determining the pattern formation time are the average cell concentration, the average swimming speed of the bacteria, and their rate of consuming oxygen.

## II. EXPERIMENTS

The mass density of organisms, algae, and bacteria that generate bioconvection varies from 2% to 15% greater than that of water. The mean local density $\overline{\rho}$ of the suspension is

$$\overline{\rho} = \rho_w + (\rho_c - \rho_w) n V, \tag{1}$$

where $\rho_w$ and $\rho_c$ are the densities of water and organisms, $V$ is the volume of one organism, and $n$ is the concentration (number of organisms per volume of the suspension). The volume fraction is then $\Phi = nV$.

In this paper the organism studied is the wild-type YB 886 strain of the bacterium *Bacillus subtilis*, a gram-positive, endospore-forming, aerobic eubacterium commonly found in soils. For a well mixed, stationary phase of a culture of these cells, $\Phi \lesssim (10^9\,\mathrm{cm}^{-3}) \times (10^{-12}\,\mathrm{cm}^3)$. The cells are rod shaped, $0.7\,\mu$m in diameter; the length varies, but is usually in the range $2–6\,\mu$m. The swimming speed within one nominally uniform culture varies widely also, typically $\lesssim 60\,\mu\mathrm{m\ s}^{-1}$, with a mean of $\sim 20\,\mu\mathrm{m\,s}^{-1}$ [15].

The motion of the bioconvection rolls, or plumes, is dissipative. To maintain this motion, the suspended organisms must swim upwards, on average, to generate gravitational

 

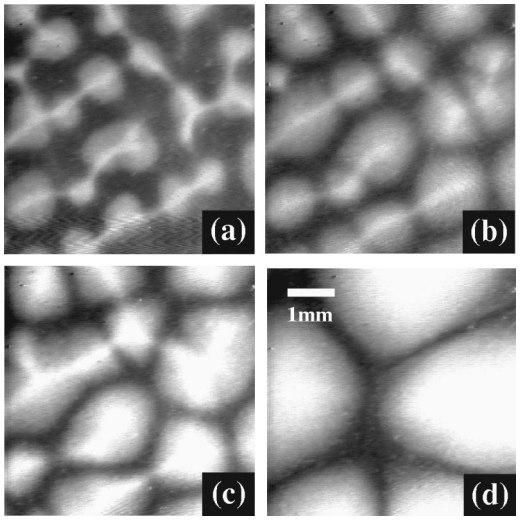


FIG. 1. Plan view of pattern formation in a petri dish containing a shallow suspension of bacteria. A section of $5.5\times5.5\,\mathrm{mm}^2$ is shown. The series (a)–(d) illustrates states (v)–(vii) of bioconvection (see text). The pictures are made by dark-field photography, i.e., the brightness increases proportionally to cell concentration.

potential energy. The relative upward swimming can occur anywhere in the fluid, as the organisms are advected with it. When the swimmers are gyrotactic, i.e., upward directed by gravity and concurrently rotated by vorticity, there is often no upward accumulation of organisms [10].

*Bacillus subtilis* consume oxygen, i.e., they are aerobic. When suspended in a relatively deep layer of fluid (e.g., 1 mm), their oxygen consumption lowers the oxygen concentration in the water. However, oxygen diffuses in from the air-water interface above. The cells within range sense the oxygen concentration gradient, swim up it, and therefore accumulate near the top of the fluid. This accumulation is equivalent to an increase of $\overline{\rho}$. In this situation, bioconvection begins as a gravitational (Rayleigh-Taylor) instability. During fully developed bioconvection, oxygen-charged water from the interface convects downward, so that bacteria swim toward a complex convection-dependent gradient.

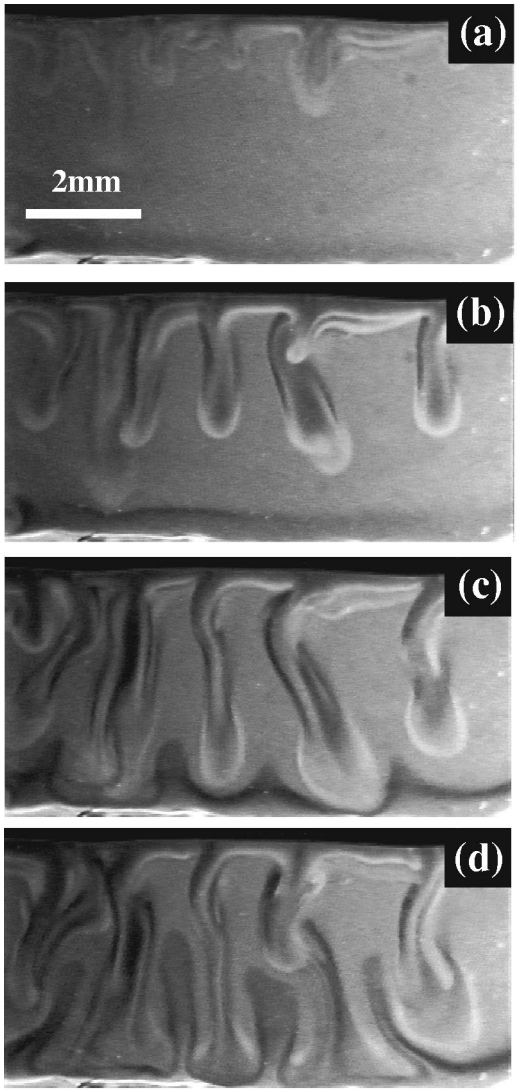


FIG. 2. Side view of pattern formation in a thin upright container. The wall-to-wall distance is 1.2 mm. The series (a)–(d) approximately illustrates the states (iv)–(vii) of bioconvection (see text). The details differ from the case shown in Fig. 1, since the geometry is quite different.

### A. From instability to steady bioconvection

This paper presents results due of a method for analyzing the onset of the gravitational instability, and its transition to approximately steady bioconvection. In order to interpret the quantitative analysis of the experiments, the progress of the initial instability can be described as a sequence of states partially illustrated in Figs. 1 and 2.

(i) A well-mixed initial state.

(ii) An oxygen concentration gradient develops; no response initially, then bacteria swim up-gradient.

(iii) Bacteria accumulate at the air-water interface. There is no visible instability (i.e., variations in cell concentration).

(iv) Near the top of the fluid the concentrated, relatively high mass density layer of bacteria ''wrinkles'' due to the gravitational instability. Descending regions contain many cells; because of incompressibility they ''pull'' the surrounding upper layers of fluid, thereby strengthening the instability.

(v) The plumes descend, and the extra cells drawn into them increase opacity in bright field, or increase scattering (whiteness) in dark field visualization.

(vi) Plumes hit bottom and spread, as a typical gravity current; upwelling fluid compensates for descending plumes.

(vii) Steady bioconvection is approached. The wavelength changes from that characterizing the ''onset,'' i.e., gravitational instability, to one that is appropriate for steady bioconvection [16]. The geometry and symmetry also changes accordingly.

The method employed for analyzing part of this sequence of events consists of obtaining a top view video record of events. The contrast generated by the developing changes in (projected) cell concentration is then measured and analyzed. Thus, states (i)–(iii) in the above sequence cannot provide data; (v) yields maximum contrast; and (vi), leading to (vii), characterizes the onset of the steady nonlinear regime that develops from the spread of the plumes' feet to generation of rolling convection.

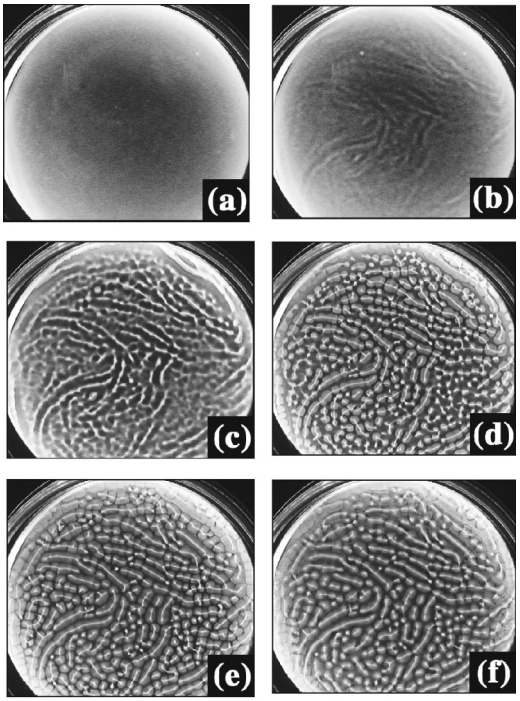


FIG. 3. Macroscopic plan view of pattern formation in a petri dish of diameter $d=5.2$ cm, at a suspension height $h=1.28$ mm. The average optical density was $0.85\pm0.05$ at 600 nm, which corresponds to a cell concentration $n\approx 6\pm 2\times 10^8$ cells/cm$^3$. White regions indicate high cell densities (dark field photography). The appropriate time instants from (a) to (f) are indicated in Fig. 4.

### B. Optical density

The index of refraction of bacterial cells is not the same as that of water; there is also absorption. The light incident on a cell culture is therefore absorbed and scattered. The intensity along the path of a light beam that shines through a suspension of organisms decreases. Off-angle observation reveals the scattered light. When the initial intensity of light passing in the $z$ direction through a suspension of depth $h$ is $I_0$, the relative intensity $I_h$ emerging after passage is given by [17,18]

$$\ln\frac{I_h}{I_0}=-\int_0^h \epsilon n(z')dz'. \tag{2}$$

The $\log_{10}$ version is called ''optical density,'' or OD. The extinction coefficient $\epsilon$ includes absorption and scattering. For well mixed suspensions in a standard container, the OD is proportional to $n$. Equation (2) assumes single scattering. For dark-field photography, as in Figs. 1–3, the observed intensity $I_k$ is proportional to the scattered light, i.e.,

$$I_k\sim I_0-I_h=I_0\left(1-\exp\left[-\int_0^h \epsilon_s n(z')dz'\right]\right),$$

where $\epsilon_s$ is the scattering part of the extinction coefficient at the angle of observation. When $h$ and $n(z)$ are sufficiently small,

$$I_k\sim I_0(1-\exp[-\epsilon_s\overline{n}h])\approx I_0\epsilon_s\overline{n}h.$$

Thus $I_k/I_0$ is approximately proportional to the $z$-averaged mean organism concentration $\overline{n}(x,y)$. It should be noted that, since the organisms are rod shaped, their orientation affects $\epsilon_s$ at a given angle of observation. To generate a substantial effect, this phenomenon would require collective alignment of the local cell population. We found no evidence of such an occurrence during our experiments.

Because of the plan-view projection, there is no observable change in $\int_0^h \epsilon_s n(z')dz'$ during states (i), (ii), and (iii), even though $n(z)$ progressively increases upwards. However, in states (iv) and (v), the effective value of the integral becomes much greater at a plume since it contains the high concentration of cells that are descending from the surface.

### C. Data evaluation

The typical pattern formation time is in the order of minutes. During this short period the total cell population, i.e., the overall average cell concentration can be considered as constant. However, in an interval of 1–2 h (the typical run of our experiments) this constancy may not hold. To follow the changes in the cell population, we repeatedly measured the the optical density of the suspension with a standard photometer (Bausch & Lomb Spec 21) at a wavelength of 600 nm.

The video records were analyzed using a Silicon Graphics workstation with a built in video capture board. The resolution of the digitized pictures was $N=640\times 480$ pixels with 256 gray levels. The standard American video system (NTSC) provides 30 images per second, which determines the maximum sampling rate. One cycle of pattern formation runs typically 2–3 min. First, the starting time of a cycle was defined by observing the cessation of visible macroscopic motion left over from mixing. The average over 30 subsequent images of the first second was used to create a reference background. A sampling rate of 1 frame/s was used for the subsequent image processing, since the characteristic time of pattern formation is much longer than $\frac{1}{30}$ s. Difference images were created by subtracting the gray level values of the pixels of the background obtained at the beginning of each run. This process eliminated the problems arising from inhomogeneities in the illumination. To characterize the time evolution of the global system, we measured the standard deviation $\sigma$ which is defined as

$$\sigma=\sqrt{\frac{1}{N-1}\sum_{j=1}^{N} g_j^2}, \tag{3}$$

where $g_j$ is the gray level value of the $j$th pixel in the difference image, and $j$ goes over all the $N$ pixels. An increasing $\sigma$ indicates increasing grayness difference between the light and dark regions of an evolving pattern.

## III. EXPERIMENTAL RESULTS

### A. Delay time measurement

Figure 3 illustrates a typical time evolution of macroscopic pattern formation. The characteristic pattern composed of irregularly arranged plumes emerges at about the same time throughout the fluid layer, rather like a photo during development. Its form is apparently not correlated with the container geometry, except at the edges where wetting

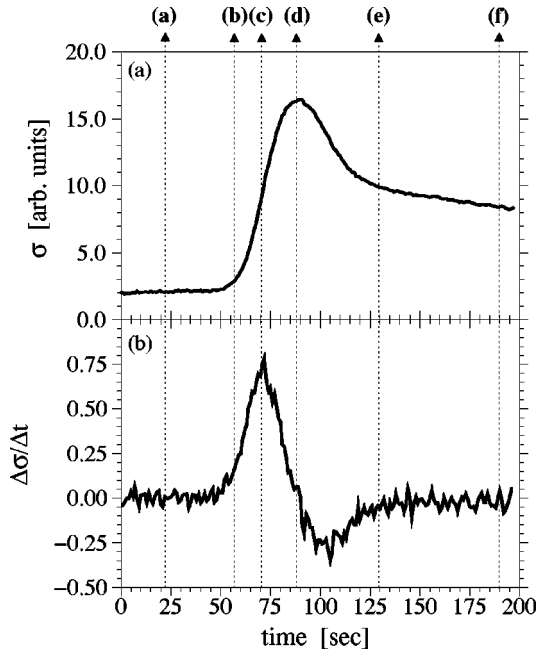


FIG. 4. Time evolution of $\sigma$ [see Eq. (3)] and its centered first neighbor numerical derivative. Characteristic points are indicated by dotted arrows, the labels (a)–(f) on the top identify the appropriate snapshots in Fig. 3.

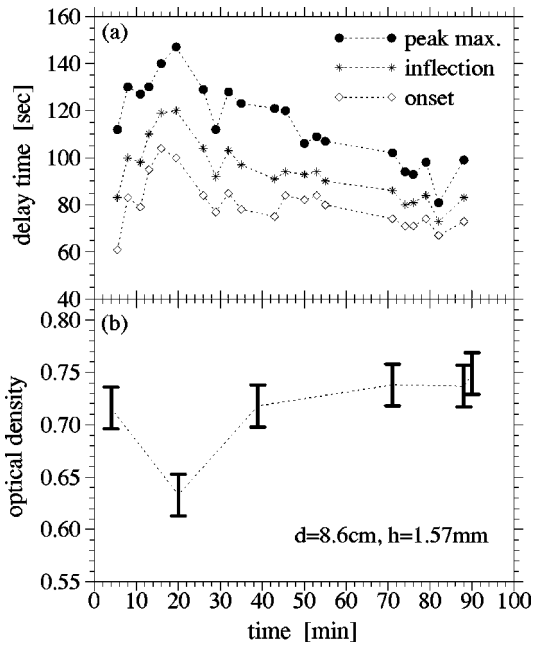


FIG. 5. (a) Delay time of the pattern formation as the function of the aging time of a given culture. Three characteristic points are evaluated from the $\sigma(t)$ curves: the onset (empty diamonds), the inflection point (stars), and the peak maximum (filled circles); see Fig. 4. (b) Average optical density of the same culture as a function of aging time. The vertical bars indicate a standard deviation.

increases depth. The pronounced irregularity implies that the pattern results from random perturbations. In spite of the level change effect near the wall, this boundary appears not to affect the interior regions, as is the case for Rayleigh-Bénard patterns with nonforcing sidewall conditions [19]. As in the case of algal bioconvection, some of the longer streaks, actually curtainlike chains of plumes, are remnants from the agitation of the fluid that precedes each experimental run.

In Fig. 4 we plot the typical time evolution of the value of $\sigma$ [see Eq. (3)], and its numerical derivative. Arrows indicate the labels and time instants belonging to the snapshots in Fig. 3. Note that the sequence covers the initial part of the pattern formation, i.e., approximately phases (i)–(vi).

Figure 4 traces the growth of the instability. The data encompass both the fluid dynamics and the distribution of microswimmers. It is somewhat surprising that the maximum contrast $\sigma_{\max}$ occurs at a time that matches the image Fig. 3(d), where the plumes have started to spread as gravity currents along the bottom of the petri dish. This stage also corresponds to Figs. 1(a) and 1(b). The cells spreading along the bottom increase mean grayness, or reduce $\sigma$. Evidently the still sharpening plumes compensate for that effect, yielding a maximum in $\sigma$. Further correlation of Figs. 1, 3, and 4 are left to the reader. The method of $\sigma$ measurement clearly provides a tool for investigating in detail the initial stages of bioconvection.

Figure 5 shows the results of repeated experiments with a given culture. The suspension of bacteria was placed in a petri dish of diameter $d=8.6$ cm. At its center the height of the liquid layer was $h=1.57$ mm. The swirling-waiting cycles were repeated several times; the records were evaluated in the way described above. Figure 5(a) shows the pattern formation time, or delay time, as a function of the aging of the culture. This interval was measured from the instant when the suspension was poured into the petri dish. Figure 5(b) shows the time development of the optical density.

The optical density was obtained by filling the suspension from the petri dish into a Bausch & Lomb test tube, and gently shaking to homogenize the suspension before the measurement. The standard deviation of the optical density values is estimated from repeated readouts after repeated shaking.

The nonmonotonic time evolution of the optical density in Fig. 5 occurs occasionally. It is caused by some of the bacteria sticking to the surfaces of a new petri dish. Usually the population grew continuously (see Figs. 6 and 7). These particular results are shown, because they illustrate the strong correlation between the pattern formation time and the average cell concentration: At higher populations the delay time is shorter.

Figure 5(a) suggests that the main source of error in the measured delay time is the uncertainties in the initial condition. The fine structure of the curves for the three characteristic points are almost identical, and the short-time fluctuations cannot be attributed to similarly short-time fluctuations of the overall cell concentration. The initial configurations were prepared by swirling the petri dish for 10 s. Remaining inhomogeneities and perhaps visually undetectable slow flows may have resulted in a relatively large measurement error. These problems, and intermittent sticking of organisms to container walls, limit the accuracy of experiments with bacteria.

### B. Absence of size effects

What are the effects of different dish sizes and filling heights on the pattern formation time? As for the dish diam-

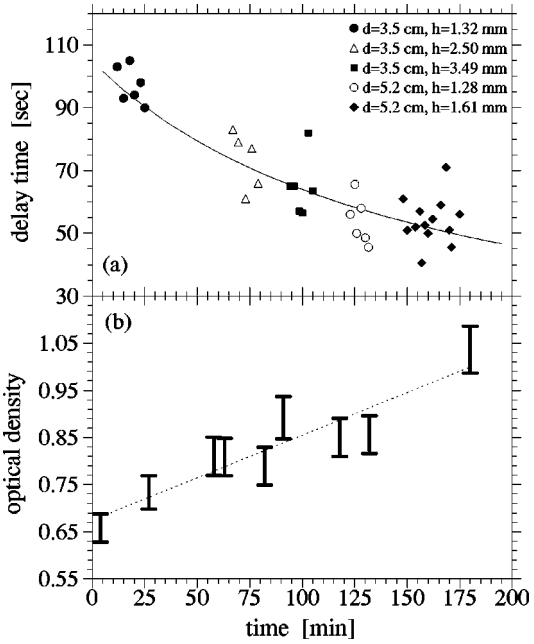


FIG. 6. (a) Delay time of the pattern formation as a function of aging time of a culture. The inflection points of the $\sigma(t)$ curves are plotted (cf. Figs. 4 and 5). Experiments were performed in different petri dishes at different filling heights; see the legends. The fitted solid line shows an inverse time dependence. (b) Average optical density of the same culture as a function of aging time. The dotted line is the least square fit.

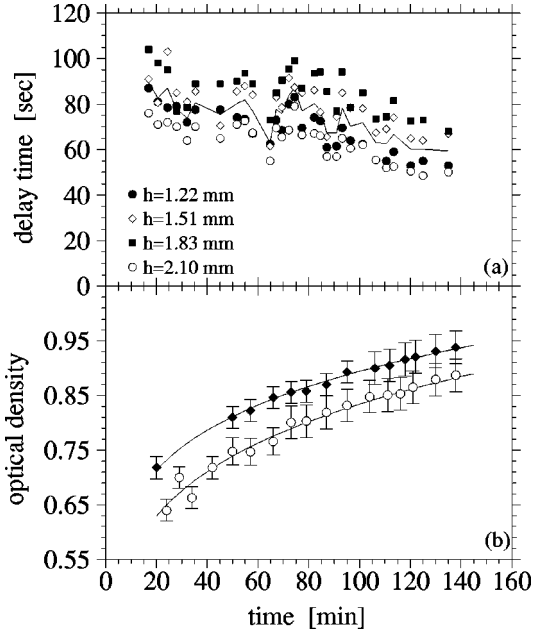


FIG. 7. (a) Delay time of the pattern formation as a function of the aging time measured simultaneously at four different filling heights $h$; see the legends. The inflection points of the $\sigma(t)$ curves are plotted (see Fig. 2). The thin solid line shows the average of the four measured values. (b) Average optical density of the control culture (empty circles) and the base culture agitated on a shaker table (heavy diamonds) as a function of aging time. The solid lines are empirical power-law fits.

eter $d$, we do not expect any significant dependence because of the lack of long range wall effects, i.e., the lack of correlations between the size and geometry of the dish and the morphology of the patterns. The dependence on the filling height $h$ is analyzed in Sec. IV. One may guess that if the pattern forming instability is based on simple mass inversion, the delay time should not depend on $h$ at high enough cell densities. Figure 6 shows the results of an experiment with a single source culture put into two petri dishes with different diameters and different filling heights. A monotonic decrease of the delay time as a function of aging time is observed, while the average cell concentration increases roughly linearly. Note that a significant dependence on the filling height would imply that the last two data sets in Fig. 6(a) (empty circles and filled diamonds) should have values much closer to the first set (filled circles) than they actually have (cf. the filling heights $h$).

In order to check further the dependence on $h$, we performed replicated experiments in a special container having four identical wells of diameter $d=3.4$ cm in a square frame. Various volumes of the base culture were filled into these containers and the delay times and optical densities were measured as before. The time evolution of the optical density was tracked by measuring a control culture in a separate petri dish of the same size. This suspension was taken from the same base culture as the others under the camera. Moreover, the control dish was held on the recording table as well, in order to approximate the circumstances in the measuring dishes (illumination, mixing, etc.) as closely as possible. This method was necessary because the small quantity of the suspension in the measuring dishes would have made difficult a sufficiently accurate density measurement. We also measured the optical density of the base culture held in a side arm flask on a shaker table. The results are plotted in Fig. 7.

The correlation between a globally decreasing delay time and increasing average density is apparent again. The fine structure of the curves belonging to different filling heights shows strong similarities indicating again the problems of preparing and defining properly an initial configuration. It is easy to recognize systematic differences between the four pattern formation times, which could suggest a dependence on filling heights. In fact, the two curves running below the average (heavy and empty circles) belong to the shallowest and deepest filling heights, respectively. Furthermore, at the end of the experiments we measured the final optical densities and observed a higher value in these two dishes by $\sim 5\%$.

The base culture held on a shaker table had systematically much higher cell densities than that of the control culture [Fig. 7(b)]. This may relate to aeration, but since the slopes are similar, it is likely that different initial concentrations cause the offset.

## IV. ANALYSIS

A continuum model for bioconvection in a suspension of aerotactic cells requires a set of equations including the Navier-Stokes and mass-conservation equations of hydrodynamics, as well as a reaction-diffusion equation for the oxygen concentration. Detailed mathematical analysis on the development of concentration gradients was performed by Hillesdon and co-workers [11,14]. They assumed a constant average cell concentration, because their analysis is focused on the short-time behavior starting from a well-stirred, ho-

mogeneous initial configuration. Thus a direct comparison of their predictions with our measurements is difficult. Instead of using the same (rather complex) formulation of the full problem, here we present simplified estimates and computer simulations on an assembly of noninteracting aerotactic swimmers.

Let us first summarize the key variables of the model. Initially, we have a uniform suspension of cells, average concentration $n_0$, in a finite layer of height $h$. Typical values are $n_0=10^7$–$10^9$ cells/cm$^3$, and $h=1$–$3$ mm. The liquid is bounded by the bottom of a container at $z=0$, the surface at $z=h$ has contact with the ambient air. The bacteria swim up a gradient of oxygen concentration $\nabla c(z)$ which they generate by consuming oxygen with a rate of $k=10^6$ molecules/cell/s [20]. At the top of the layer the concentration of oxygen is in equilibrium with the atmosphere; $c(h)=c_0 \approx 10^{17}$ molecules/cm$^3$. The diffusivity of oxygen is $D=2\times10^{-5}$ cm$^2$/s, which limits the diffusive supply below the top layer.

Pattern formation in our system appears to be initiated by a Rayleigh-Taylor-type instability [13,21], which is a fingering or ''wrinkling'' instability of an interface between two fluids of different densities. An analogy with the Rayleigh-Bénard instability is also pertinent [4,9,11,14]. The basic physical control parameter is the density difference $\Delta\rho=\rho_H-\rho_L$, where $\rho_H$ characterizes the fluid of higher density overlaying a fluid of lower density $\rho_L$. The magnitude $\Delta\rho$, for the onset of bioconvection ought to be similar to the density between top and bottom water layers at the onset of the ''usual'' Rayleigh-Bénard convection. For example, in a layer of distilled water at a depth of $h=3.18$ mm the calculated density difference is $\Delta\rho\approx6.5\times10^{-4}$ g/cm$^3$ [22]. Estimating a cell volume of 2 $\mu$m$^3$ and an excess density of 10% for *Bacillus subtilis*, Eq. (1) gives an excess concentration of cells in the top layer of $\Delta n\approx3\times10^9$ cells/cm$^3$. This excess concentration is built up by the upward flux of swimming cells halted by the impenetrable air-fluid interface.

### Estimates of upward self-concentration

Upward accumulation is due to the mean directional component $\overline{v}$ of swimming velocity along the gradient of oxygen molecules, generated by consumption and supply. The process is characterized by three distinct time scales that can be estimated separately, but which actually overlap to some extent. A characteristic length scale $(h-z^*)$ also emerges.

The upswimming time from a given depth $z^*$ to the vicinity of the fluid-air boundary is

$$t_{\rm swim}(z^*)=\int_{z^*}^{h-\lambda}\frac{dz}{\overline{v}(z)}. \tag{4}$$

When $\overline{v}(z)$, the average upward speed is $\overline{v}$, a constant, $t_{\rm swim}(z^*)\approx(h-z^*)/\overline{v}$. The thickness $\lambda\ll(h-z^*)$ of the layer of cells concentrated near the top surface can be estimated from the boundary condition that requires that the total flux $j(z)$ of swimming organisms [6] vanish at $z=h$. The random swimming motion can be modeled by a cell diffusion coefficient $D_c\approx v_0 l/3$, where $v_0$ is the mean swimming speed, and $l$ is the mean length of an approximately straight swimming path, sandwiched between random changes in direction, as in kinetic gas theory [20]. Then

$$j(z)=n(z)\overline{v}-D_c\frac{dn(z)}{dz}. \tag{5}$$

Setting $j(z)=0$ at $z=h$,

$$\frac{dn}{n}=\frac{\overline{v}dz}{D_c}\equiv\frac{dz}{\lambda}. \tag{6}$$

If $\overline{v}\approx v_0$, $\lambda\approx l/3$, or about 30 $\mu$m, if $l\approx100$ $\mu$m, a guess based on observations. The exact value of $\lambda$ is not important, as long as $\lambda\ll(h-z^*)$.

A standard measure for the diffusive penetration time of the oxygen to the level $z^*$ is $t_{\rm grad}\approx(h-z^*)^2/2D$. Cells at $z>z^*$ sense the direction from which oxygen is supplied, and swim, with mean spead $\overline{v}$, toward the source, the air-water interface. Below $z^*$ the organisms experience no directional stimulus. Their swimming is randomly oriented and ever slower as the initially available oxygen of concentration $c_0$ is consumed [15].

The time for depletion of oxygen is $t_{\rm dep}=c_0/(n_0k)$. Setting $t_{\rm grad}=t_{\rm dep}$ yields $(h-z^*)=\sqrt{2c_0D/(n_0k)}$, and also $t_{\rm swim}$. For numerical estimates we use $c_0=10^{16}$ molecules/cm$^3$, $n_0=10^8$ bacteria/cm$^3$, and $\overline{v}=2\times10^{-3}$ cm/s. The results are $(h-z^*)=6\times10^{-2}$ cm, which is much greater than $\lambda$. Also $t_{\rm dep}=100$ s and $t_{\rm swim}=30$ s. The net accumulation time $T\approx t_{\rm dep}+t_{\rm swim}=130$ s, which corresponds well both to the experimentally observed and numerically simulated times for the onset of instability. These estimates show self-consistency and consistency with both the experimental results and the numerical simulation, to be presented.

Finally, an estimate is required for the cell concentration, and mass density offset within the organism-rich layer near the top of the fluid. Conservations of organisms requires that

$$\lambda n_\lambda(t)=n_0(h-z^*(t)), \tag{7}$$

where $n_\lambda(t)$ is the concentration of cells within $h-\lambda\leqslant z\leqslant h$ at time $t$, and $z^*(t)$ is given by inverting Eq. (4). Given the above numerical estimates, one obtains $n_\lambda(T)\approx2\times10^9$ bacteria/cm$^3$, equivalent to a mean separation of $\sim10$ $\mu$m in qualitative agreement with microscope observations. Because lack of oxygen causes the cessation of swimming, most of the bacteria in the region $z<z^*$ at $t=0$ remain there, when $z^*$ is found by setting $t_{\rm grad}=t_{\rm dep}$, as above. A few cells do make it $z>z^*$, by random swimming, but this number is likely to be negligible. Some, perhaps 10%, of the cells within $z^*<z<(h-\lambda)$ do not swim up the oxygen gradient.

Using Eqs. (4) and (7) to eliminate $z^*$, and assuming $\overline{v}=$const, one finds that

$$t_{\rm swim}(z^*)\equiv T=\frac{\lambda n_\lambda}{\overline{v}n_0}. \tag{8}$$

Then, from Eq. (1),

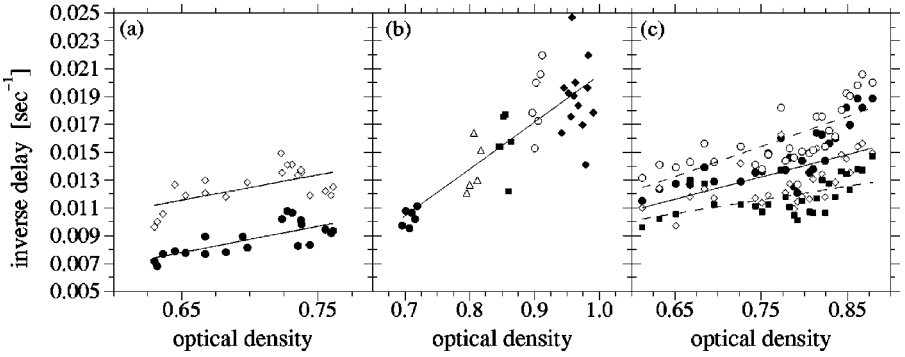


FIG. 8. (a) Inverse delay time for pattern formation as function of optical density. Two sets from Fig. 5(a) are shown; the symbols are identical. The linear fits have slopes $0.019\pm0.002$ (empty diamonds) and $0.018\pm0.002$ (filled circles). (b) The same as (a), for the data of Fig. 6(a). The slope is $0.034\pm0.003$. (c) The same as (a), for the data of Fig. 7(a). The solid line shows a fit for the average with a slope $0.016\pm0.003$. Dashed lines show the largest and smallest fitted slopes for the individual sets with values $0.023\pm0.002$ and $0.013\pm0.003$.

$$T=\frac{\lambda}{v}\frac{\overline{\rho_\lambda}-\rho_w}{\rho_0-\rho_w}. \tag{9}$$

The time $T$ can be identified with the time for reaching a critical value for $\overline{\rho_\lambda}$. Equation (8) shows that $\lambda$ enters as $\lambda n_\lambda$, i.e., as a conserved cell number. These equations also show that $T$ is independent of the fluid height $h$, in agreement with our experimental results Figs. 6 and 7. Furthermore, $T$ is inversely proportional to the initial uniform cell concentration $n_0$. Figure 8 plots all of the experimental data shown before, as a function of the optical density. The data appear to agree qualitatively with the predictions.

The experimental resolution is obviously not too good. The upward trend of the data is consistent with proportionality to $n_0$. The difference between the slopes in Fig. 8(b), compared with Figs. 8(a) and 8(c), suggests that bacteria in the culture used for the experimental series shown in Fig. 6 might have swum twice as fast as the others. Swimming speed may be correlated with rate of concentration increase, a subject for future investigation.

It would be useful, for guiding future measurements and analyses, to compute the sensitivity of $T$ to various facts or assumptions about the relationships between the fundamental set of parameters $\{n_0,\overline{v},k,\ldots\}$ and also the probability densities for speed and direction of swimming. As a first step, a simple numerical model was constructed to investigate the concept.

The numerical simulations model density stratification due to upward swimming of the bacteria, in the oxygen gradient generated by consumption and supply. The simulations do not extend into the onset of hydrodynamic instability; furthermore hydrodynamical interactions between the swimmers are not involved. We consider a finite volume of suspension. Periodic boundary conditions are imposed in the horizontal direction. At the beginning we place randomly a given number of ''aerotactic walkers'' in the volume. The random initial coordinates have a uniform distribution. The number of walkers is kept fixed in a simulational run (cell conservation). A given initial oxygen profile is also prescribed with a constant or depth-dependent concentration $c(z)$. Oxygen is represented by bookkeeping the number of molecules in the volume. Coarse-grained cell and oxygen densities are calculated for horizontal slices of height $\Delta z=50\,\mu$m. In the case of a uniform oxygen distribution, the walkers isotropically move around in random directions, and consume oxygen. The dynamics is the following. We ''measure'' the oxygen concentration and its gradient at the height of a given particle. If the gradient is strong enough (typically $\sim10^{13}$ molecules/cm$^4$), the walker is directed upward with an average velocity $v_0=20\,\mu$m/s. After taking into account the boundary conditions, the position of each particle is updated. During the replacement the consumption of oxygen with the rate $k=10^6$ molecules/cell/s is calculated. After evaluating the consumption, the supply is modeled by solving a coarse-grained diffusion equation with a standard numerical method [23]. After getting the new oxygen profile, the next iteration follows.

Figure 9 shows numerically derived relationships between $T$ and optical density for various adjustments of the parameters governing a large number of oxygen consuming, gradient-sensing ''organisms.'' As in the experiments and subsequent analysis, there is an inverse relationship between $T$ and $n_0$. Further work on this approach is in progress; it will be reported at a later date.

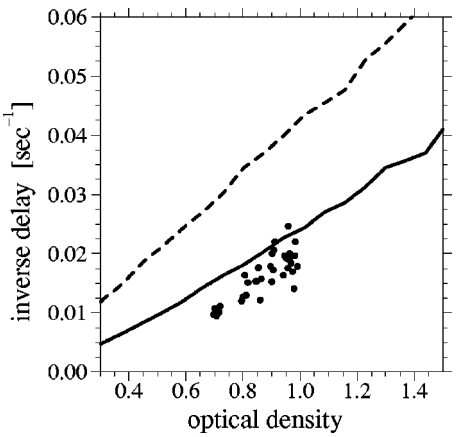


FIG. 9. Inverse delay time as a function of optical density: Numerical simulations. The heavy dots are the experimental values from Fig. 8(b). The solid line is the simulation result assuming a uniform initial oxygen distribution. For the dashed line, an *ab initio* oxygen gradient was the initial condition.

## V. SUMMARY

In the past analytical and computational models based on various idealizations of micro-organism behavior and fluid mechanics were used to investigate the characteristic features of bioconvection patterns driven by geotactic and gyrotactic algae and aerotactic bacteria. These results were related qualitatively to experimental observations. Some remarkable two-dimensional many-organism simulations have recently been completed by Fauci and Hopkins [24]. These simulations included fluid and organism dynamics. They were not quantitatively related to experiments, although they did demonstrate complex dynamics very similar to observed ones. Bees and Hill [16] applied Fourier methods to the analysis of inception and growth of experimentally observed algal bioconvection patterns. Given these antecedents, the results presented in this paper cover new ground, to our knowledge, combining quantitative analysis of experiments and modeling of these remarkable complex systems.

(1) We have developed a powerful method, based on the standard deviation of optical density, for analyzing quantitatively the sequential stages of bioconvection. They are upward accumulation to criticality, lateral hydrodynamic concentration into plumes, and evolution of the strongly nonlinear convective regime.

(2) Results of relatively naive but robust analytical methods match the observed dependence of the delay times $T$ on cell concentration and independence on container dimensions.

(3) Numerical simulations also found inverse correlation between the time $T$ and the the concentration of organisms.

These satisfactory results pave the way toward more detailed local and global analyses of bioconvection patterns, and to simulations that will employ experimentally derived aerotactic sensitivities as well as probability densities for swimming velocities [15]. We then expect to provide insights into the relation between the behaviors of various species of organisms and the dynamics which they elicit.

## ACKNOWLEDGMENTS

This work was supported by NATO Collaborative Research Grant No. CRG-960634, and by the Hungarian National Science Foundation (OTKA) under Grant Nos. F26645 and F17310. I. M. J. thanks the Foundation for Research and Higher Education for their financial support. J. O. K. gratefully acknowledges the support of Alice and Ralph Sheets, via a grant to the University of Arizona Foundation.

[1] J. R. Platt, Science **133**, 1766 (1961).
[2] M. S. Plesset and H. Winet, Nature (London) **248**, 441 (1974).
[3] T. J. Pedley and J. O. Kessler, Sci. Prog. **76**, 105 (1992).
[4] S. Childress, M. Levandowsky, and E. A. Spiegel, J. Fluid Mech. **63**, 591 (1975).
[5] J. O. Kessler, Nature (London) **313**, 218 (1985).
[6] J. O. Kessler, Contemp. Phys. **26**, 147 (1985).
[7] J. O. Kessler, J. Fluid Mech. **173**, 191 (1986).
[8] N. A. Hill, T. J. Pedley, and J. O. Kessler, J. Fluid Mech. **208**, 509 (1989).
[9] T. J. Pedley and J. O. Kessler, J. Fluid Mech. **212**, 155 (1990).
[10] T. J. Pedley and J. O. Kessler, Annu. Rev. Fluid Mech. **24**, 313 (1992).
[11] A. J. Hillesdon, T. J. Pedley, and J. O. Kessler, Bull. Math. Biol. **57**, 299 (1995).
[12] J. O. Kessler and N. A. Hill, in *Physics of Biological Systems: From Molecules to Species*, edited by H. Flyvbjerg *et al.* (Springer-Verlag, Heidelberg, 1997).
[13] R. V. Vincent and N. A. Hill, J. Fluid Mech. **327**, 343 (1996).
[14] A. J. Hillesdon and T. J. Pedley, J. Fluid Mech. **324**, 223 (1996).
[15] J. O. Kessler and M. F. Wojciechowski, in *Bacteria as Multicellular Organisms*, edited by J. A. Shapiro and M. Dworkin (Oxford University Press, New York, 1997), p. 417.
[16] M. A. Bees and N. A. Hill, J. Exp. Biol. **200**, 1515 (1997).
[17] C. F. Bohren and D. R. Huffmann, *Absorbtion and Scattering of Light by Small Particles* (Wiley, New York, 1983).
[18] A. L. Koch, J. Theor. Biol. **18**, 133 (1970).
[19] Ch. W. Meyer, G. Ahlers, and D. S. Cannell, Phys. Rev. Lett. **59**, 1577 (1987).
[20] H. C. Berg, *Random Walks in Biology* (Cambridge University Press, Cambridge, 1983).
[21] D. H. Sharp, Physica D **12**, 3 (1984).
[22] Ch. W. Meyer, G. Ahlers, and D. S. Cannell, Phys. Rev. A **44**, 2514 (1991).
[23] W. H. Press, S. A. Teukolsky, W. T. Vetterling, and B. P. Flannery, *Numerical Recipes*, 2nd ed. (Cambridge University Press, Cambridge, 1992).
[24] L. J. Fauci and M. Hopkins (private communication).